


MAY 05 2020

Three-dimensional dislocations in a uniform linear array's isotropic sensors—Direction finding's hybrid Cramér-Rao bound ✓

Zakayo Ndiku Morris  ; Kainam Thomas Wong  ; Yue Ivan Wu



J. Acoust. Soc. Am. 147, 3209–3220 (2020)

<https://doi.org/10.1121/10.0001138>



Articles You May Be Interested In

A uniform circular array of isotropic sensors that stochastically dislocate in three dimensions—The hybrid Cramér-Rao bound of direction-of-arrival estimation

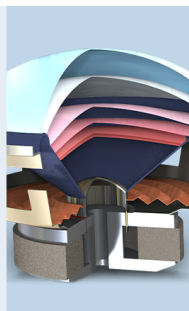
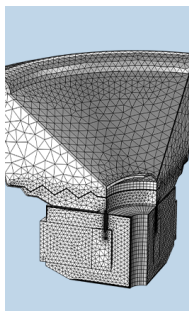
J. Acoust. Soc. Am. (July 2019)

Hybrid Cramér-Rao bound of direction finding, using a triad of cardioid sensors that are perpendicularly oriented and spatially collocated

J. Acoust. Soc. Am. (August 2019)

Rules-of-thumb to design a uniform spherical array for direction finding—Its Cramér-Rao bounds' nonlinear dependence on the number of sensors

J. Acoust. Soc. Am. (February 2019)



COMSOL

Find your best idea
with multiphysics modeling
and simulation apps

« LEARN MORE

Three-dimensional dislocations in a uniform linear array's isotropic sensors—Direction finding's hybrid Cramér-Rao bound

Zakayo Ndiku Morris,^{1,a)} Kainam Thomas Wong,^{2,b)} and Yue Ivan Wu^{3,c)}

¹Department of Electronic and Information Engineering, Hong Kong Polytechnic University, Hong Kong, China

²School of General Engineering, Beihang University, Beijing, China

³College of Computer Science, Sichuan University, Chengdu, China

ABSTRACT:

The linear array's *one*-dimensional spatial geometry is simple but suffices for *univariate* direction finding, i.e., is adequate for the estimation of an incident source's direction-of-arrival relative to the linear array axis. However, this nominal *one*-dimensional ideality could be often physically compromised in the real world, as the constituent sensors may dislocate *three*-dimensionally from their nominal positions. For example, a towed array is subject to ocean-surface waves and to oceanic currents [Tichavsky and Wong (2004). IEEE Trans. Sign. Process. **52**(1), 36–47]. This paper analyzes how a nominally linear array's *one*-dimensional direction-finding accuracy would be degraded by the *three*-dimensional random dislocation of the constituent sensors. This analysis derives the hybrid Cramér-Rao bound (HCRB) of the arrival-angle estimate in a closed form expressed in terms of the sensors' dislocation statistics. Surprisingly, the sensors' dislocation could improve and not necessarily degrade the HCRB, depending on the dislocation variances but also on the incident source's arrival angle and the signal-to-noise power ratio.

© 2020 Acoustical Society of America. <https://doi.org/10.1121/10.0001138>

(Received 23 November 2019; revised 3 April 2020; accepted 6 April 2020; published online 5 May 2020)

[Editor: James F. Lynch]

Pages: 3209–3220

I. INTRODUCTION

For sensor-array direction finding, the uniform linear array (ULA) geometry [please see Fig. 1(a)] is one of the commonest spatial geometries. Table 1 samples practical implementations of the uniform linear array, including two commercially available products (XMOS, 2018; Barbagelata *et al.*, 2008).

The open literature offers many investigations on the direction-finding performance of a linear array of uniformly spaced identical isotropic sensors (like hydrophones or microphones). Specifically, the corresponding Cramér-Rao bound (CRB) may be found in the following papers for a *perfectly* linear array.

- (1) Derived in a *closed* form in Demissie and Willett (2008), Fittipaldi and Luise (2008), Leshem and der Veen (1999), Li and Compton (1991), Stoica and Nehorai (1989), Tuncer and Friedlander (2009) [Eq. (1.148), p. 43], and Bellili *et al.* (2010).
- (2) Derived in an *open* form in Abdellatif *et al.* (2000), Agrawal and Prasad (2000), Gershman and Bohme (1997), Gershman *et al.* (2001), Xia *et al.* (2007), Ye and DeGroat (1993, 1995), Zatman (1998), and Zhenghui and Gunawan (2000).

- (3) Plotted graphically (but without showing the corresponding mathematical expressions for the Cramér-Rao bound) in Choi (2002), Fayad *et al.* (2014), Kaneko and Sano (2008), Kautz and Zoltowski (1996), Li and Lu (2007), Li *et al.* (2013), and Ottersten *et al.* (1991).

The array's nominally linear geometry and nominally uniform inter-sensor spacing, however, may be violated in field deployment, with the constituent sensors randomly dislocated from their nominal positions. For example, a towed array is subject to ocean-surface waves and to oceanic currents [Tichavsky and Wong (2004)]. Please see Fig. 1(b), which shows *three*-dimensional dislocation of one particular sensor. The three dimensions here refer to the two dimensions perpendicular to the array axis and the one dimension along the array axis.

Though any sensor could dislocate *three*-dimensionally, this fully *three*-dimensional case has never had its Cramér-Rao bound derived, plotted, or analyzed in the open literature. Instead:

- (A) Dislocation *one*-dimensionally only *along* the array axis is mentioned in passing in VanTrees and Bell (2007) (p. 32) as a possible sensor-dislocation model, but has not been investigated in any way therein. In thus modeling the dislocation as *only* along the array axis, the array's linear geometry is maintained, though the inter-sensor spacings' uniformity is allowed violation.
- (B) Dislocation only *perpendicularly* to the array axis (Hinich, 1977; Schultheiss and Ianniello, 1980; Wong *et al.*, 1988).

^{a)}ORCID: 0000-0001-5143-2485.

^{b)}ORCID: 0000-0002-1583-6682.

^{c)}Electronic mail: y.i.wu@ieec.org, ORCID: 0000-0001-5480-1741.

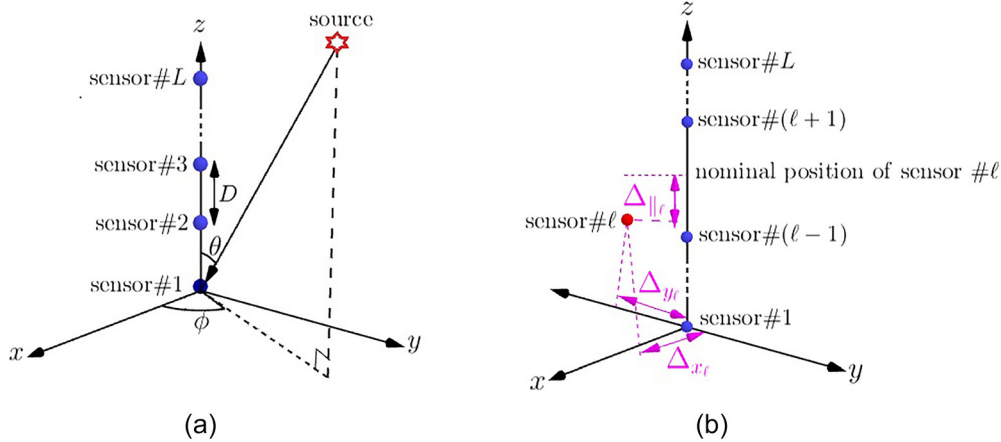


FIG. 1. (Color online) A nominally uniform linear array of L sensors, each represented by a solid blue dot. (a) All sensors lie precisely at their nominal positions. (b) Sensor $\#l$ suffers three-dimensional mislocation.

- (B-1) This perpendicular dislocation is limited to *one* dimension in [Schultheiss and Ianniello \(1980\)](#) and [Wong et al. \(1988\)](#) (despite the two dimensions of the plane perpendicular to the array axis) in the closed-form Cramér-Rao bounds derived therein.
- (B-2) This perpendicular dislocation is described in [Hinich \(1977\)](#) as *two*-dimensional, but no corresponding Cramér-Rao bound is derived nor plotted therein.
- (C) Dislocation one-dimensionally *along* the array axis plus one additional dimension *perpendicular* to the array axis ([Schultheiss and Ianniello, 1980](#); [VanTrees, 2002](#); [Wan et al., 2014](#); [Wong et al., 1988](#)).
 - (C-1) Such dislocation is mentioned in passing in [Wong et al. \(1988\)](#), but no Cramér-Rao bound is derived therein.
 - (C-2) For such dislocation, the Cramér-Rao bound is plotted in [VanTrees \(2002\)](#) (p. 1097), but no derivation is presented therein.
 - (C-3) For such dislocation, the Cramér-Rao bound is derived in open form in [Wan et al. \(2014\)](#) without giving much derivation.

TABLE I. Practical/commercial implementations of a uniform linear array of isotropic sensors.

Number of sensors	Inter-sensor spacing	Reference
4	16 cm	(Tayem et al., 2014)
4 ^a	3.333 cm	(XMOS, 2018)
7	5 cm	(Aalborg University, 2018)
8	25 cm	(Jing et al., 2018)
10	4 cm	(Hu et al., 2016)
128 ^b	49 cm	(Barbagelata et al., 2008)
not stated	not stated	(University of Pretoria, 2018)
not stated	not stated	(JSK Naval Support, 2018)

^aThis is a commercial product, “xCORE VocalFusion™ Speaker Part Number XK-VF3100-L33,” manufactured by XMOS (Bristol, United Kingdom).

^bThis is a commercial product, “Prakla 128,” manufactured by *Prakla-Seismos* (Hanover, Germany).

In summary, the abovementioned literature on a uniform linear array’s direction-finding performance offers *no* Cramér-Rao bound for *three*-dimensional sensor dislocations. This present work is first in the open literature to analyze this three-dimensional dislocation’s effects on the uniform linear array direction-finding Cramér-Rao bound.

The rest of this paper is organized as follows: Section II presents the measurement’s statistical model. Section III presents the hybrid Cramér-Rao bound (which is rigorously derived in the [Appendix](#)) and delineates its qualitative attributes. Section IV compares the special sub-cases of sensor dislocations (1) only along the array’s nominal axis, (2) only perpendicular to the array’s nominal axis, and (3) over all three spatial dimensions. Section V verifies the derived hybrid Cramér-Rao bound with Monte Carlo simulations of the corresponding maximum *a posteriori* estimation (MAP), which is well known to asymptotically approach the hybrid Cramér-Rao bound. Section VI concludes the entire investigation.

II. MEASUREMENT STATISTICAL MODEL

A. For a perfectly uniform linear array

Consider a linear array of L identical isotropic sensors, positioned on the positive z -axis with a prior known uniform inter-sensor spacing of $D \in (0, \lambda/2]$. Please see Fig. 1(a).

The resulting $L \times 1$ array manifold (a) would have an ℓ th entry of $[\mathbf{a}]_{\ell} = e^{j\gamma_{\ell}}$, where

$$\gamma_{\ell} = (\ell - 1)2\pi \frac{D}{\lambda} \cos(\theta), \quad (1)$$

where λ refers to the prior known wavelength of the incident signal.

B. For a nominally uniform linear array whose sensors may dislocate only along the array axis

A sensor may deviate from its nominal position in the real world.

If the ℓ th sensor's dislocation is limited to merely along the array axis, Eq. (1) would become (VanTrees and Bell, 2007, p. 32)

$$\gamma_\ell = 2\pi \left[(\ell - 1) \frac{D}{\lambda} + \frac{\Delta_{\parallel,\ell}}{\lambda} \right] \cos(\theta). \quad (2)$$

This paper's subsequent analysis will model $\Delta_{\parallel,\ell}$ as stochastic, Gaussian, zero-mean, having a variance of $\sigma_{\Delta_{\parallel}}^2$, with all entries in $\{\Delta_{\parallel,1}, \Delta_{\parallel,2}, \dots, \Delta_{\parallel,L}\}$ statistically independent of each other and with all other data-model entities.

C. For a nominally uniform linear array whose sensors may dislocate only perpendicularly to the array axis

If the ℓ th sensor's dislocation is limited to only perpendicular to the array axis, then $\Delta_{\parallel,\ell} = 0$ and Eq. (1) would become

$$\gamma_\ell = \frac{2\pi}{\lambda} \{ \Delta_{x,\ell} \sin(\theta) \cos(\phi) + \Delta_{y,\ell} \sin(\theta) \sin(\phi) + (\ell - 1)D \cos(\theta) \}. \quad (3)$$

In the above, $\Delta_{x,\ell}$ represents the ℓ th sensor's dislocation along the x axis. This paper's subsequent analysis will model these dislocation parameters as stochastic, Gaussian, zero-mean, with a variance of $\sigma_{\Delta_{\perp}}^2$. Similar descriptions hold for $\Delta_{y,\ell}$. Lastly, $\{\Delta_{x,1}, \dots, \Delta_{x,L}, \Delta_{y,1}, \dots, \Delta_{y,L}\}$ forms a statistically independent set.¹

If, furthermore, $\Delta_{y,\ell} = 0$, then²

$$\gamma_\ell = \frac{2\pi}{\lambda} \{ \Delta_{x,\ell} \sin(\theta) \cos(\phi) + (\ell - 1)D \cos(\theta) \}. \quad (4)$$

The one-dimensional perpendicular dislocation of Schultheiss and Ianniello (1980) and Wong *et al.* (1988) is thereby obtained.

D. For a nominally uniform linear array whose sensors may dislocate in three-dimensional space

Each sensor's dislocation could in general be three-dimensional in practice, not necessarily only along the array axis nor only perpendicular of the array axis.

This three-dimensional dislocation has been neglected in the open literature, but can be modeled as follows:

$$\gamma_\ell = \frac{2\pi}{\lambda} \left\{ \Delta_{x,\ell} \sin(\theta) \cos(\phi) + \Delta_{y,\ell} \sin(\theta) \sin(\phi) + [(\ell - 1)D + \Delta_{\parallel,\ell}] \cos(\theta) \right\}. \quad (5)$$

Here, $\{\Delta_{x,1}, \dots, \Delta_{x,L}, \Delta_{y,1}, \dots, \Delta_{y,L}, \Delta_{\parallel,1}, \dots, \Delta_{\parallel,L}\}$ forms a statistically independent set.

To ease subsequent derivation, define the $3L \times 1$ vector,

$$\Delta := [\Delta_{x,1}, \dots, \Delta_{x,L}, \Delta_{y,1}, \dots, \Delta_{y,L}, \Delta_{\parallel,1}, \dots, \Delta_{\parallel,L}]^T,$$

where the superscript T symbolizes transposition.

This paper's subsequent analysis will model all entries in $\{\Delta_{x,\ell}, \Delta_{y,\ell}, \Delta_{\parallel,\ell}, \forall \ell\}$ as stochastic, Gaussian, zero-mean,

and statistically independent of each other. Moreover, $\Delta_{x,\ell}$ and $\Delta_{y,\ell}$ have a same variance of $\sigma_{\Delta_{\perp}}^2$ for all ℓ , whereas $\Delta_{\parallel,\ell}$ has a common variance of $\sigma_{\Delta_{\parallel}}^2$ for all ℓ .

III. THE DERIVED HYBRID CRAMÉR-RAO BOUND FOR A NOMINALLY UNIFORM LINEAR ARRAY WHOSE SENSORS MAY DISLOCATE IN THREE-DIMENSIONAL SPACE

For direction finding using a nominally linear array of uniformly spaced identical isotropic sensors which nonetheless may stochastically dislocate from their nominal positions, the Appendix has analytically derived the hybrid Cramér-Rao bound under three-dimensional dislocation (for the first time in the open literature):

$$\begin{aligned} \text{HCRB}_{\parallel,\perp}(\theta) &= \frac{1}{LM \left[2\pi \frac{\sigma_s}{\sigma_n} \right]^2} \left\{ 2 \left[\frac{\sigma_{\Delta_{\perp}}}{\lambda} \cos(\theta) \right]^2 + 2 \left[\frac{\sigma_{\Delta_{\parallel}}}{\lambda} \sin(\theta) \right]^2 \right. \\ &\quad \left. + \frac{\frac{1}{3} \left[\frac{D}{\lambda} \sin(\theta) \right]^2 (L-1)(2L-1)}{M \left(2\pi \frac{\sigma_s}{\sigma_n} \right)^2 \left[\left(\frac{\sigma_{\Delta_{\perp}}}{\lambda} \sin(\theta) \right)^2 + \left(\frac{\sigma_{\Delta_{\parallel}}}{\lambda} \cos(\theta) \right)^2 \right] + 1} \right\}^{-1} \\ &= \left\{ \text{SNR}_{\text{eff}} L \left[2a_{\text{ext}} \left(\frac{\sigma_{\Delta_{\parallel}}}{\lambda}, \frac{\sigma_{\Delta_{\perp}}}{\lambda}, \theta \right) \right. \right. \\ &\quad \left. \left. + \frac{\left[\frac{D}{\lambda} \sin(\theta) \right]^2 (L-1)(2L-1)}{3 \left(2\text{SNR}_{\text{eff}} a_{\text{nui}} \left(\frac{\sigma_{\Delta_{\parallel}}}{\lambda}, \frac{\sigma_{\Delta_{\perp}}}{\lambda}, \theta \right) + 1 \right)} \right] \right\}^{-1}, \end{aligned} \quad (6)$$

where

$$\text{SNR}_{\text{eff}} := M \left(2\pi \frac{\sigma_s}{\sigma_n} \right)^2$$

represents the effective signal-to-noise power ratio, and

$$\begin{aligned} a_{\text{ext}} \left(\frac{\sigma_{\Delta_{\parallel}}}{\lambda}, \frac{\sigma_{\Delta_{\perp}}}{\lambda}, \theta \right) &:= \left(\frac{\sigma_{\Delta_{\perp}}}{\lambda} \cos(\theta) \right)^2 + \left(\frac{\sigma_{\Delta_{\parallel}}}{\lambda} \sin(\theta) \right)^2 \\ &\geq 0, \\ a_{\text{nui}} \left(\frac{\sigma_{\Delta_{\parallel}}}{\lambda}, \frac{\sigma_{\Delta_{\perp}}}{\lambda}, \theta \right) &:= \left(\frac{\sigma_{\Delta_{\perp}}}{\lambda} \sin(\theta) \right)^2 + \left(\frac{\sigma_{\Delta_{\parallel}}}{\lambda} \cos(\theta) \right)^2 \\ &= a_{\text{ext}} \left(\frac{\sigma_{\Delta_{\parallel}}}{\lambda}, \frac{\sigma_{\Delta_{\perp}}}{\lambda}, \theta \pm \frac{\pi}{2} \right) \\ &\geq 0. \end{aligned}$$

The above $\text{HCRB}_{\parallel,\perp}(\theta)$ in Eq. (6) contains six degrees of freedom: L , SNR_{eff} , D/λ , $\sigma_{\Delta_{\parallel}}/\lambda$, $\sigma_{\Delta_{\perp}}/\lambda$, and θ .

The following qualitative trends may be observed of the $\text{HCRB}_{\parallel,\perp}(\theta)$ of Eq. (6).

- (i) $\text{HCRB}_{\parallel,\perp}(\theta)$ is independent of ϕ , despite that the Fisher information matrix's every entry [except the (1, 1)th entry] depends on ϕ . This functional independence of Eq. (6) from ϕ is intuitively reasonable, because the sensors' dislocation statistics is rotationally symmetric with respect to the z -axis.
- (ii) $\text{HCRB}_{\parallel,\perp}(\theta)$ decreases (i.e., improves) monotonically with an increasing SNR_{eff} , with all else kept constant. This trend would become obvious by re-expressing Eq. (6) as

$$\begin{aligned}\text{HCRB}_{\parallel,\perp}(\theta) &= \left\{ \gamma_1 \text{SNR}_{\text{eff}} \left[\gamma_2 + \frac{\gamma_3}{\gamma_4 \text{SNR}_{\text{eff}} + 1} \right] \right\}^{-1} \\ &= \left\{ \gamma_1 \text{SNR}_{\text{eff}} [\gamma_2 \gamma_4 \text{SNR}_{\text{eff}} + \gamma_2 + \gamma_3] \right\}^{-1} \\ &\quad + \gamma_4 \{ \gamma_1 [\gamma_2 \gamma_4 \text{SNR}_{\text{eff}} + \gamma_2 + \gamma_3] \}^{-1},\end{aligned}$$

where $\gamma_1, \gamma_2, \gamma_3, \gamma_4$ are all independent of SNR_{eff} .

- (iii) $\text{HCRB}_{\parallel,\perp}(\theta)$ decreases (i.e., improves) monotonically with an increasing L , as all else remain the same. This trend would become obvious by examining Eq. (6), which may be expressed as

$$\text{HCRB}_{\parallel,\perp}(\theta) = \{ L \beta_1 [\beta_2 + \beta_3 (L-1)(2L-1)] \}^{-1}, \quad (7)$$

where $\beta_1, \beta_2, \beta_3$ are all independent of L . This trend is also intuitively expected, because a larger aperture can resolve the direction-of-arrival more finely. Indeed, as $L \rightarrow \infty$, $\text{HCRB}_{\parallel,\perp}(\theta)$ approaches zero.³

- (iv) $\text{HCRB}_{\parallel,\perp}(\theta)$ decreases (i.e., improves) as the non-negative $(D/\lambda)\sin(\theta)$ increases. The latter is directly proportional to the nominally linear array's spatial aperture size projected onto the incident wavefront. This direct relationship between $\text{HCRB}_{\parallel,\perp}(\theta)$ and $(D/\lambda)\sin(\theta)$ is thus unsurprising. As $(D/\lambda)\sin(\theta) \rightarrow 0$, $\text{HCRB}_{\parallel,\perp}(\theta) \rightarrow \{ 2a_{\text{ext}}((\sigma_{\Delta\parallel}/\lambda), (\sigma_{\Delta\perp}/\lambda), \theta) \text{LSNR}_{\text{eff}} \}^{-1}$.⁴
- (v) $\text{HCRB}_{\parallel,\perp}(\theta)$ decreases (i.e., improves) with a larger $a_{\text{ext}}(\sigma_{\Delta\parallel}/\lambda, \sigma_{\Delta\perp}/\lambda, \theta)$. This latter expression corresponds to the sensors' dislocation *along* the wavefront (as opposed to perpendicular to the wavefront). This dislocation *along* the wavefront would enlarge (over the sensor dislocation's "probability space" as a whole) the array's effective aperture along the wavefront. This explains why $\text{HCRB}_{\parallel,\perp}(\theta)$ decreases as the aforementioned expression increases.
- (vi) $\text{HCRB}_{\parallel,\perp}(\theta)$ decreases (i.e., improves) with a *smaller* $a_{\text{nui}}(\sigma_{\Delta\parallel}/\lambda, \sigma_{\Delta\perp}/\lambda, \theta)$. This latter expression corresponds to the sensors' dislocation *perpendicular* to the wavefront, hence no effect on the array's effective aperture along the wavefront. Nonetheless, the sensors' dislocations are nuisance parameters that degrade the hybrid Fisher information matrix; this

expression could be construed to embody these nuisance parameters' statistical degradation of the Fisher information. This explains why $\text{HCRB}_{\parallel,\perp}(\theta)$ decreases as the aforementioned expression decreases.

- (vii) SNR_{eff} amplified the positive effects of the sensors' dislocation identified above in (v), and reduces the negative effects identified in (vi).
- (viii) The contrary effects in (v) and (vi) have magnitudes dependent also on the incident source's arrival angle.

IV. SPECIAL CASE: DISLOCATION STOCHASTICS IS ISOTROPIC

Suppose that the sensor dislocation variance is same along all Cartesian directions (i.e., same whether parallel or perpendicular to the linear array axis). That is, $\sigma_{\Delta\perp}^2 = \sigma_{\Delta\parallel}^2 = \sigma_{\Delta}^2$. Then, Eq. (6) simplifies to

$$\begin{aligned}\text{HCRB}_{\parallel,\perp}(\theta) &= \frac{1}{\text{LSNR}_{\text{eff}}} \\ &\quad \times \left[2 \left(\frac{\sigma_{\Delta}}{\lambda} \right)^2 + \frac{\frac{1}{3} \left(\frac{D}{\lambda} \right)^2 \sin^2(\theta) (L-1)(2L-1)}{2 \left(\frac{\sigma_{\Delta}}{\lambda} \right)^2 \text{SNR}_{\text{eff}} + 1} \right]^{-1}.\end{aligned} \quad (8)$$

This simplified expression has only four degrees-of-freedom: SNR_{eff} , L , $(D/\lambda)\sin(\theta)$, σ_{Δ}/λ —versus the six earlier in the most general case of Eq. (6).

Figure 2 gives a typical plot of Eq. (8), i.e., the figure would remain roughly the same for other values of L and SNR_{eff} . Please see also Fig. 3(a).

How $\text{HCRB}_{\parallel,\perp}(\theta)$ varies with SNR_{eff} and with L —which was described, respectively, in points (ii)–(iii) of Sec. III.

As to how $\text{HCRB}_{\parallel,\perp}(\theta)$ varies with $(D/\lambda)\sin(\theta)$ and with σ_{Δ}/λ —please refer to Fig. 2. There, the following may be observed:

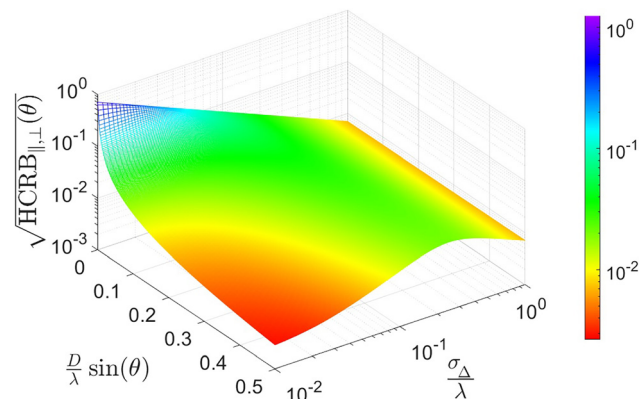


FIG. 2. (Color online) $\text{HCRB}_{\parallel,\perp}(\theta)$ of Eq. (7) plotted versus σ_{Δ}/λ and versus $(D/\lambda)\sin(\theta)$, at $L = 10$ and $\text{SNR}_{\text{eff}} M(\sigma_s/\sigma_n)^2 = 10$.

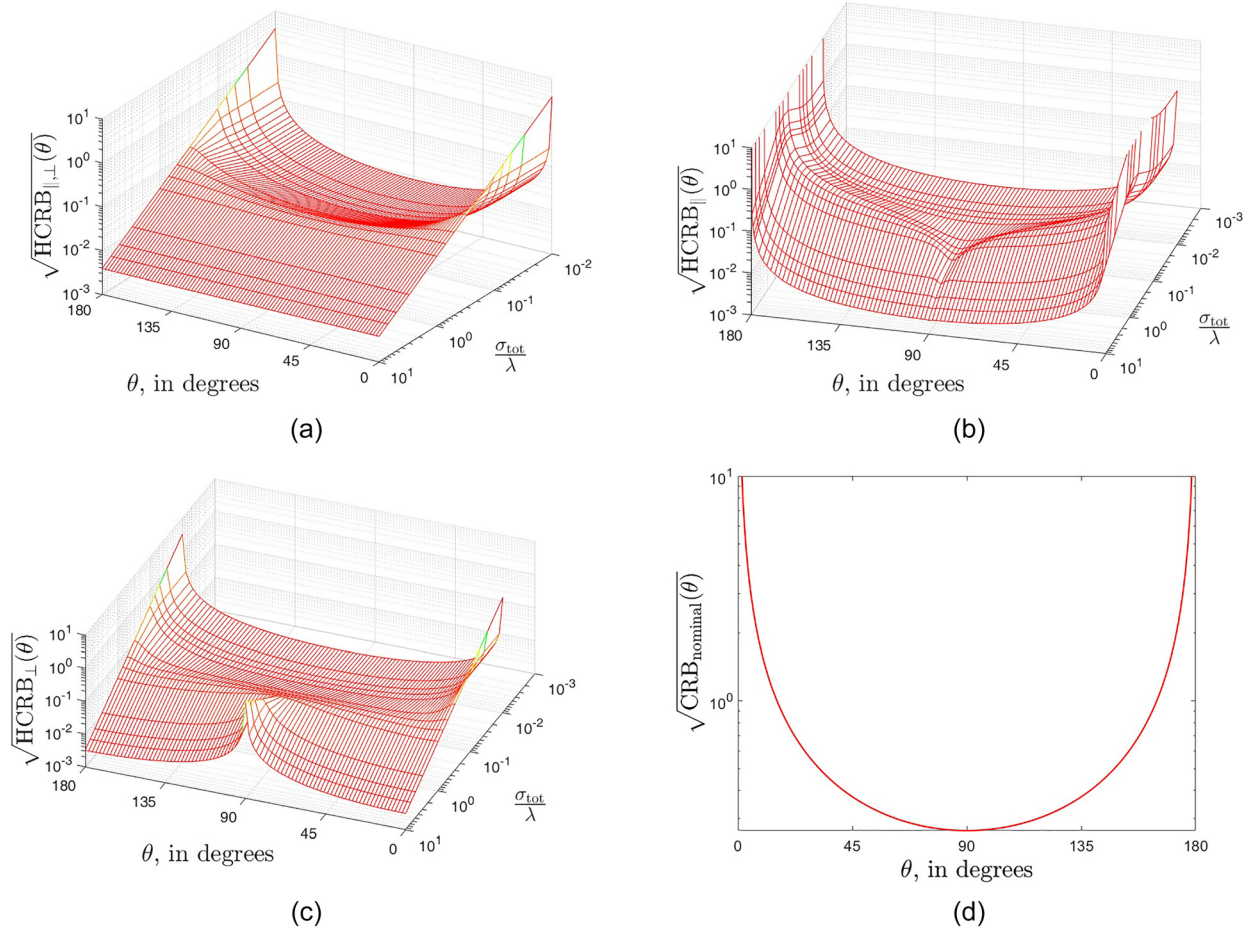


FIG. 3. (Color online) Here, $L = 10$, $\text{SNR}_{\text{eff}} = 100$, and $D/\lambda = \frac{1}{2}$. (a) $\text{HCRB}_{\parallel,\perp}(\theta)$ of Eq. (8). This case has σ_{tot}^2 distributed isotropically in three-dimensional Cartesian space, hence $\sigma_{\Delta}/\lambda = (1/\sqrt{3})(\sigma_{\text{tot}}/\lambda)$. (b) $\text{HCRB}_{\parallel}(\theta)$ of Eq. (9). This case has σ_{tot}^2 distributed only along the array axis, hence $\sigma_{\Delta}/\lambda = \sigma_{\text{tot}}/\lambda$. (c) $\text{HCRB}_{\perp}(\theta)$ of Eq. (10). This case has σ_{tot}^2 distributed omnidirectionally on a two-dimensional Cartesian plane that is normal to the array axis, hence $\sigma_{\Delta}/\lambda = (1/\sqrt{2})(\sigma_{\text{tot}}/\lambda)$. (d) $\text{CRB}_{\text{nominal}}(\theta)$ of Eq. (11).

- (ix) As $\sigma_{\Delta}/\lambda \rightarrow \infty$, $\text{HCRB}_{\parallel,\perp}(\theta) \rightarrow 0$, implying possibly no estimation error for an unbiased estimator. This result might be surprising, but is explainable on account of the infinitely large aperture consequential of $\sigma_{\Delta}/\lambda \rightarrow \infty$.
- (x) The hybrid Cramér-Rao bound increases (i.e., worsens) with an increasing σ_{Δ}/λ up to a local maximum but decreases thereafter.⁵ This is due to the contrary effects from $a_{\text{ext}}(\sigma_{\Delta}/\lambda, \sigma_{\Delta\perp}/\lambda, \theta)$ versus from $a_{\text{nui}}(\sigma_{\Delta}/\lambda, \sigma_{\Delta\perp}/\lambda, \theta)$, as already explained under points (v)–(vii) in Sec. III. Both of these factors vary with θ ; hence, the peak's coordinates of $(\sigma_{\Delta}/\lambda, \sigma_{\Delta\perp}/\lambda)$ vary with θ .
- (xi) $\text{HCRB}_{\parallel,\perp}(\theta)$ decreases as the direction-of-arrival θ increases from 0 toward $\pi/2$, i.e., as the signal's incident direction becomes more perpendicular to the linear array axis. Intuitively, this is because as $\theta \rightarrow \pi/2$, the impinging wavefront would be received by an effective aperture that has widened. Mathematically in Eq. (6), the denominator is dominated by $\sin(\theta)$ which increases as $\theta \rightarrow \pi/2$, thereby decreasing $\text{HCRB}_{\parallel,\perp}(\theta)$. Indeed, the $\text{HCRB}(\theta)$ in Fig. 2

decreases at a faster rate, as θ approaches 0, as $\sin(\theta)$ drops more quickly toward zero as $\theta \rightarrow 0$.

A. Special case: For a nominally uniform linear array whose sensors may dislocate *only* along the array axis

With $\sigma_{\Delta\perp} = 0$, Eq. (6) simplifies to

$$\text{HCRB}_{\parallel}(\theta) = \frac{\csc^2(\theta)}{L\text{SNR}_{\text{eff}}} \left[2 \left(\frac{\sigma_{\Delta\parallel}}{\lambda} \right)^2 + \frac{\frac{1}{3} \left(\frac{D}{\lambda} \right)^2 (L-1)(2L-1)}{2\text{SNR}_{\text{eff}} \left(\frac{\sigma_{\Delta\parallel}}{\lambda} \right)^2 \cos^2(\theta) + 1} \right]^{-1}. \quad (9)$$

This expression has not appeared in any earlier reference, though VanTrees and Bell (2007) (p. 32) mentioned this

dislocation model in passing. This expression is plotted in Fig. 3(b). The cliffs (at $\theta = 0, 180^\circ$) arise due to the $\csc^2(\theta)$ multiplicative factor in Eq. (9). A trough appears for small $\sigma_{\Delta\parallel}/\lambda$ at $\theta = 90^\circ$ due to the $(\sigma_{\Delta\parallel}/\lambda)^2 \cos^2(\theta)$ factor in Eq. (9).

B. Special case: The derived hybrid Cramér-Rao bound if $\sigma_{\Delta\parallel} = 0$

If $\sigma_{\Delta\parallel}^2 = 0$, Eq. (6) simplifies to

$$\text{HCRB}_\perp(\theta) = \frac{1}{\text{LSNR}_{\text{eff}}} \left[2 \left(\frac{\sigma_{\Delta\perp}}{\lambda} \right)^2 \cos^2(\theta) + \frac{\frac{1}{3} \left(\frac{D}{\lambda} \sin(\theta) \right)^2 (L-1)(2L-1)}{2\text{SNR}_{\text{eff}} \left(\frac{\sigma_{\Delta\perp}}{\lambda} \right)^2 \sin^2(\theta) + 1} \right]^{-1}. \quad (10)$$

This expression has not appeared in any earlier reference, although this dislocation model was mentioned in Hinich (1977) and a one-dimensional perpendicular dislocation model was mentioned in Schultheiss and Ianniello (1980) and Wong *et al.* (1988). This expression is plotted in Fig. 3(c). The ridge for very large $\sigma_{\Delta\parallel}/\lambda$ at $\theta = 90^\circ$ reflects the $\cos^2(\theta)$ in the denominator's first term inside the square brackets in Eq. (10).

C. Special case: For a perfectly uniform linear array

If all sensors are located exactly at their nominal positions, it would hold that $\sigma_{\Delta\perp}^2 = \sigma_{\Delta\parallel}^2 = \sigma_{\Delta}^2 = 0$. Then, Eq. (6) degenerates to

$$\text{CRB}_{\text{nominal}}(\theta) = \frac{3\csc^2(\theta)}{\text{SNR}_{\text{eff}} L(L-1)(2L-1)} \left(\frac{D}{\lambda} \right)^{-2}. \quad (11)$$

This expression equals the Cramér-Rao bound [Li and Compton (1991), Eq. (21); Bellili *et al.*, 2010, Eq. (24); Tuncer and Friedlander (2009), Eq. 1.148, p. 43].

D. Special case: Comparing the various special cases

Compare the along-axis dislocation versus the perpendicular dislocation; which is more damaging? To answer this question, set $\sigma_{\Delta\parallel} = \sigma_{\Delta\perp} = \sigma_{\Delta}$. Then, rewrite Eqs. (8)–(10), respectively, as

$$\text{HCRB}_{\perp,\perp}(\theta) = L^{-1} \left\{ \tilde{\sigma}_{\Delta} + \frac{\tilde{D}}{1 + \tilde{\sigma}_{\Delta}} \right\}^{-1}, \quad (12)$$

$$\text{HCRB}_{\parallel}(\theta) = L^{-1} \left\{ \tilde{\sigma}_{\Delta} \sin^2(\theta) + \frac{\tilde{D}}{1 + \tilde{\sigma}_{\Delta} \cos^2(\theta)} \right\}^{-1}, \quad (13)$$

$$\begin{aligned} \text{HCRB}_\perp(\theta) &= L^{-1} \left\{ \tilde{\sigma}_{\Delta} \cos^2(\theta) + \frac{\tilde{D}}{1 + \tilde{\sigma}_{\Delta} \sin^2(\theta)} \right\}^{-1} \\ &= \text{HCRB}_{\parallel} \left(\theta \pm \frac{\pi}{2} \right), \end{aligned} \quad (14)$$

where

$$\tilde{\sigma}_{\Delta} := 2\text{SNR}_{\text{eff}} \left(\frac{\sigma_{\Delta}}{\lambda} \right)^2 \geq 0,$$

$$\tilde{D} := \frac{1}{3} \text{SNR}_{\text{eff}} (L-1)(2L-1) \left(\frac{D}{\lambda} \sin(\theta) \right)^2 \geq 0.$$

This $(L-1)(2L-1)((D/\lambda)\sin(\theta))^2$ is related positively to the projection of the array aperture onto the incident wavefront. This \tilde{D} could be construed to correspond to the incident signal's power flux through the array aperture.

Comparing the sensors' two configurations of dislocation,

$$\begin{aligned} \text{HCRB}_\perp(\theta) - \text{HCRB}_{\parallel}(\theta) &= \frac{1}{L} [\sin^2(\theta) - \cos^2(\theta)] \\ &\times \left(\frac{1}{4} \tilde{\sigma}_{\Delta}^3 \sin^2(2\theta) + (1 + \tilde{D}) \tilde{\sigma}_{\Delta} + \tilde{\sigma}_{\Delta}^2 \right) \\ &\times \left[\frac{1}{4} \tilde{\sigma}_{\Delta}^2 \sin^2(2\theta) + \tilde{\sigma}_{\Delta} \cos^2(\theta) + \tilde{D} \right]^{-1} \\ &\times \left(\frac{1}{4} \tilde{\sigma}_{\Delta}^2 \sin^2(2\theta) + \tilde{\sigma}_{\Delta} \sin^2(\theta) + \tilde{D} \right)^{-1}. \end{aligned} \quad (15)$$

Hence, $\text{HCRB}_\perp(\theta) > \text{HCRB}_{\parallel}(\theta)$, iff $\sin^2(\theta) > \cos^2(\theta)$, which in turn is equivalent to the incident polar angle $\pi/4 < \theta < 3\pi/4$. Similarly, $\text{HCRB}_\perp(\theta) < \text{HCRB}_{\parallel}(\theta)$, iff $\sin^2(\theta) < \cos^2(\theta)$, which in turn is equivalent to the incident polar angle $\{0 \leq \theta < \pi/4\} \cup \{3\pi/4 < \theta \leq \pi\}$. This may be understood intuitively as follows: As the incident signal's arrival direction is more aligned with the horizontal plane (i.e., as $\theta \rightarrow \pi/2$), a sensor dislocated more perpendicularly to the vertical array axis would more disrupt the array's nominally linear geometry, thereby compromising the estimate to a larger extent, hence the inequalities above.

As $\sigma_{\text{tot}}/\lambda$ increases and as $\theta \rightarrow \pi/2$, each sensor's horizontal displacement overshadows the nominal vertical inter-sensor spacing. The inter-sensor phase differences become so dominated by the phase difference due to the horizontal displacements and is so "randomized," to give little useful information on the direction-of-arrival.

At small $\sigma_{\text{tot}}/\lambda \ll 1$, $\text{HCRB}_{\perp,\perp}(\theta)$, $\text{HCRB}_{\parallel}(\theta)$, and $\text{HCRB}_\perp(\theta)$ all resemble $\text{CRB}_{\text{nominal}}(\theta)$.

V. MAXIMUM A POSTERIORI ESTIMATION TO VERIFY THE DERIVED HYBRID CRAMÉR-RAO BOUND

The maximum *a posteriori* (MAP) estimation maximizes the posterior probability density function of $[\theta, \Delta]$ given the observation $\tilde{\mathbf{z}}$. MAP estimation asymptotically approaches the hybrid Cramér-Rao bound [see Sec. IV on p. 2079 of Noam and Messer (2009)].

Consider the posterior probability density function of (θ, Δ) given the observation $\tilde{\mathbf{z}}$,

$$p(\theta, \Delta | \tilde{\mathbf{z}}) \propto p(\tilde{\mathbf{z}} | \theta, \Delta) p(\theta, \Delta),$$

where

$$p(\tilde{\mathbf{z}} | \theta, \Delta) = \frac{1}{|\pi \mathbf{\Gamma}|} \exp \left\{ -[\tilde{\mathbf{z}} - \mathbf{s} \otimes \mathbf{a}]^H \mathbf{\Gamma}^{-1} [\tilde{\mathbf{z}} - \mathbf{s} \otimes \mathbf{a}] \right\}$$

denotes the conditional probability density of $\tilde{\mathbf{z}}$ conditioned on (θ, Δ) , and

$$\begin{aligned} p(\Delta) &= \left(\prod_{\ell=1}^L \frac{1}{\sqrt{2\pi\sigma_{\Delta_{\perp}}^2}} e^{-\Delta_{x,\ell}^2/2\sigma_{\Delta_{\perp}}^2} \right) \\ &\times \left(\prod_{\ell=1}^L \frac{1}{\sqrt{2\pi\sigma_{\Delta_{\perp}}^2}} e^{-\Delta_{y,\ell}^2/2\sigma_{\Delta_{\perp}}^2} \right) \\ &\times \left(\prod_{\ell=1}^L \frac{1}{\sqrt{2\pi\sigma_{\Delta_{\parallel}}^2}} e^{-\Delta_{\parallel,\ell}^2/2\sigma_{\Delta_{\parallel}}^2} \right) \\ &= \left(\frac{1}{2\pi\sigma_{\Delta_{\perp}}^2} \right)^L \left(\frac{1}{2\pi\sigma_{\Delta_{\parallel}}^2} \right)^{L/2} \\ &\times \exp \left\{ -\frac{1}{2} \sum_{\ell=1}^L \left[\frac{1}{\sigma_{\Delta_{\perp}}^2} (\Delta_{x,\ell}^2 + \Delta_{y,\ell}^2) + \frac{\Delta_{\parallel,\ell}^2}{\sigma_{\Delta_{\parallel}}^2} \right] \right\} \end{aligned}$$

refers to the prior probability density function of Δ .

Hence,

$$\begin{aligned} p(\theta, \Delta | \tilde{\mathbf{z}}) &= p(\tilde{\mathbf{z}} | \theta, \Delta) p(\Delta) \\ &= \frac{1}{|\pi \mathbf{\Gamma}|} \left(\frac{1}{2\pi\sigma_{\Delta_{\perp}}^2} \right)^L \left(\frac{1}{2\pi\sigma_{\Delta_{\parallel}}^2} \right)^{L/2} \\ &\times \exp \left\{ -\left[\frac{1}{\sigma_n^2} [\tilde{\mathbf{z}} - \mathbf{s} \otimes \mathbf{a}]^H [\tilde{\mathbf{z}} - \mathbf{s} \otimes \mathbf{a}] \right. \right. \\ &\left. \left. + \frac{1}{2} \sum_{\ell=1}^L \left(\frac{1}{\sigma_{\Delta_{\perp}}^2} (\Delta_{x,\ell}^2 + \Delta_{y,\ell}^2) + \frac{\Delta_{\parallel,\ell}^2}{\sigma_{\Delta_{\parallel}}^2} \right) \right] \right\}. \end{aligned}$$

The MAP estimate of (θ, Δ) equals

$$\begin{aligned} (\hat{\theta}, \hat{\Delta}) &= \arg \max_{\{\theta, \Delta\}} p(\theta, \Delta | \tilde{\mathbf{z}}) \\ &= \arg \max_{\{\theta, \Delta\}} p(\tilde{\mathbf{z}} | \theta, \Delta) p(\Delta) \\ &= \arg \min_{\{\theta, \Delta\}} \left\{ \frac{1}{\sigma_n^2} [\tilde{\mathbf{z}} - \mathbf{s} \otimes \mathbf{a}]^H [\tilde{\mathbf{z}} - \mathbf{s} \otimes \mathbf{a}] \right. \\ &\quad \left. + \frac{1}{2} \sum_{\ell=1}^L \left(\frac{1}{\sigma_{\Delta_{\perp}}^2} (\Delta_{x,\ell}^2 + \Delta_{y,\ell}^2) + \frac{\Delta_{\parallel,\ell}^2}{\sigma_{\Delta_{\parallel}}^2} \right) \right\}. \quad (16) \end{aligned}$$

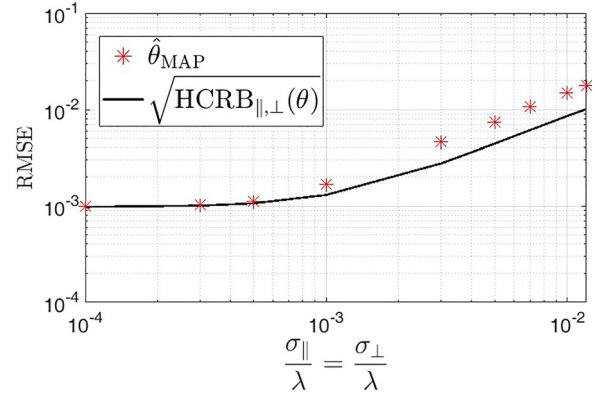


FIG. 4. (Color online) Monte Carlo simulations of the MAP estimation in Eq. (16). Each icon here is based on $N = 3000$ independent Monte Carlo trials, at the settings of $L = 30$, $M = 100$, $\sigma_s/\sigma_n = 10$, $D/\lambda = 1/2$, $\theta = 25^\circ$, $\phi = 43^\circ$, $\psi = 0.23\pi$, and $f = 0.25$.

Figure 4 presents Monte Carlo simulations of Eq. (16), showing the MAP estimator to approach the hybrid Cramér-Rao bound for asymptotically small values of $\sigma_{\Delta_{\parallel}}/\lambda$ and $\sigma_{\Delta_{\perp}}/\lambda$, thereby verifying the hybrid Cramér-Rao bound derived in Eq. (6). The root mean square error (RMSE) is defined as $\text{RMSE} = \sqrt{(1/N) \sum_{n=1}^N (\hat{\theta}_n - \theta)^2}$, where $\hat{\theta}_n$ represents the n th Monte Carlo trial's MAP polar-angle estimate.

VI. CONCLUSION

The linear array's formal *one-dimensional* ideality could be breached in implementation, with the constituent sensors dislocating *three-dimensionally* from their nominal positions. This paper has analytically derived the corresponding hybrid Cramér-Rao bound of the arrival-angle estimate in a closed form, expressed in terms of the sensors' dislocation statistics. Astonishingly to some readers perhaps, the sensors' stochastic dislocation could enhance the sensing system's direction-finding hybrid Cramér-Rao bound, due to aperture enlargement. This effect, however, is opposed by the dislocation-parameters' nuisance effects on the hybrid Fisher information matrix. These contrary influences have been theoretically analyzed, mathematically quantified, and intuitively explained in this work.

APPENDIX: DERIVATION OF THE HYBRID CRAMÉR-RAO BOUND

1. To define the data's statistical model

To focus on the sensors' dislocation, a simple statistical model is used here for the incident signal and the corrupting noise.

The incident signal is complex-valued, sinusoid, and defined as

$$s(m) := \sigma_s \exp(j(2\pi fm + \varphi)) \quad (A1)$$

at the m th time sample. Here, the amplitude σ_s , the digital frequency (also known as normalized frequency) f , and the initial phase φ are all previously known.

The additive noise is modeled as complex-valued, Gaussian, zero-mean, with a prior known variance of σ_n^2 , and spatio-temporally white.

Then, at the m th time sample, the data equals

$$\mathbf{z}(m) := \mathbf{a}s(m) + \mathbf{n}(m), \quad \forall m = 1, 2, \dots, M. \quad (\text{A2})$$

For all M time samples altogether, they may be represented in a matrix form as

$$\tilde{\mathbf{z}} := \mathbf{s} \otimes \mathbf{a} + \tilde{\mathbf{n}}, \quad (\text{A3})$$

where \otimes symbolizes the Kronecker product, and

$$\begin{aligned} \tilde{\mathbf{z}} &= [\mathbf{z}(1), \dots, \mathbf{z}(M)]^T, \\ \mathbf{s} &= [\mathbf{s}(1), \dots, \mathbf{s}(M)]^T, \\ \tilde{\mathbf{n}} &= [\mathbf{n}(1), \dots, \mathbf{n}(M)]^T. \end{aligned} \quad (\text{A4})$$

Collect all unknown parameters into a $(1 + 3L) \times 1$ vector, $\xi := [\theta, \Delta]^T$.

The conditional probability density of $\tilde{\mathbf{z}}$, conditioned on Δ is given by

$$p(\tilde{\mathbf{z}}|\Delta) = \frac{1}{\pi \Gamma} \exp \left\{ -[\tilde{\mathbf{z}} - \boldsymbol{\mu}]^H \Gamma^{-1} [\tilde{\mathbf{z}} - \boldsymbol{\mu}] \right\}, \quad (\text{A5})$$

where the superscript H symbolizes the Hermitian operator, and

$$\begin{aligned} \boldsymbol{\mu} &:= E[\tilde{\mathbf{z}}|\Delta] \\ &= \mathbf{s} \otimes \mathbf{a} + E[\tilde{\mathbf{n}}] \\ &= \mathbf{s} \otimes \mathbf{a} \end{aligned}$$

and

$$\begin{aligned} \Gamma &:= \text{cov}(\tilde{\mathbf{z}}|\Delta) \\ &= E_{\tilde{\mathbf{z}}|\Delta} \left\{ (\tilde{\mathbf{z}} - \boldsymbol{\mu})[\tilde{\mathbf{z}} - \boldsymbol{\mu}]^H \right\} \\ &= E[\tilde{\mathbf{n}}\tilde{\mathbf{n}}^H] \\ &= \sigma_n^2 \mathbf{I}_{LM \times LM}, \end{aligned}$$

where \mathbf{I} denotes an identity matrix of a size indicated in its subscript.

2. To derive the hybrid Fisher information matrix

The $(3L + 1) \times (3L + 1)$ hybrid Fisher information matrix is given by [see Eqs. (8.49)–(8.57) in VanTrees (2002)]

$$\mathbf{J} = \mathbf{J}_D + \mathbf{J}_P, \quad (\text{A6})$$

where \mathbf{J}_P represents the prior information matrix (based on prior knowledge on the dislocation variables) and \mathbf{J}_D symbolizes the information matrix due to the measured data. The (ξ_i, ξ_j) th entries of \mathbf{J}_D and \mathbf{J}_P equal

$$[\mathbf{J}_D]_{\xi_i, \xi_j} = -E_{\tilde{\mathbf{z}}|\Delta} \left[\frac{\partial^2 \ln p(\tilde{\mathbf{z}}|\Delta)}{\partial \xi_i \partial \xi_j} \right], \quad (\text{A7})$$

$$[\mathbf{J}_P]_{\xi_i, \xi_j} = -E_{\Delta} \left[\frac{\partial^2 \ln p_{\Delta}(\Delta)}{\partial \xi_i \partial \xi_j} \right], \quad (\text{A8})$$

where ξ_i denotes the i th entry of the vector parameter ξ , and $p_{\Delta}(\Delta)$ is the prior probability density function of Δ .

3. To derive \mathbf{J}_P

As Δ is zero-mean Gaussian distributed,

$$\mathbf{J}_P = \begin{bmatrix} [0.7]0 & \mathbf{0}_{1 \times 2L} & \mathbf{0}_{1 \times L} \\ \mathbf{0}_{2L \times 1} & \frac{1}{\sigma_{\Delta_{\perp}}^2} \mathbf{I}_{2L \times 2L} & \mathbf{0}_{2L \times L} \\ \mathbf{0}_{L \times 1} & \mathbf{0}_{L \times 2L} & \frac{1}{\sigma_{\Delta_{\parallel}}^2} \mathbf{I}_{L \times L} \end{bmatrix}. \quad (\text{A9})$$

If $\sigma_{\Delta_{\perp}}^2 = \sigma_{\Delta_{\parallel}}^2 = \sigma_{\Delta}^2$, Eq. (A9) becomes

$$\mathbf{J}_P = \begin{bmatrix} [0.4]0 & \mathbf{0}_{1 \times 3L} \\ \mathbf{0}_{3L \times 1} & \frac{1}{\sigma_{\Delta}^2} \mathbf{I}_{3L \times 3L} \end{bmatrix}. \quad (\text{A10})$$

4. To derive \mathbf{J}_D

From Eq. (A7) [see Eqs. (8.23)–(8.34) in VanTrees (2002)],

$$\begin{aligned} [\mathbf{J}_D]_{\xi_i, \xi_j} &= E_{\Delta} \left[2 \text{Re} \left\{ \left(\frac{\partial \boldsymbol{\mu}}{\partial \xi_i} \right)^H \Gamma^{-1} \left(\frac{\partial \boldsymbol{\mu}}{\partial \xi_j} \right) \right\} \right. \\ &\quad \left. + \text{Tr} \left\{ \Gamma^{-1} \left(\frac{\partial \Gamma}{\partial \xi_i} \right) \Gamma^{-1} \left(\frac{\partial \Gamma}{\partial \xi_j} \right) \right\} \right], \end{aligned}$$

where ξ_i denotes the i th entry of the vector ξ , but Γ is independent of ξ ; thus

$$\begin{aligned} [\mathbf{J}_D]_{\xi_i, \xi_j} &= E_{\Delta} \left[2 \text{Re} \left\{ \left(\frac{\partial \boldsymbol{\mu}}{\partial \xi_i} \right)^H \Gamma^{-1} \left(\frac{\partial \boldsymbol{\mu}}{\partial \xi_j} \right) \right\} \right] \\ &= \frac{2}{\sigma_n^2} E_{\Delta} \left[\underbrace{\text{Re} \left\{ \left(\frac{\partial \boldsymbol{\mu}}{\partial \xi_i} \right)^H \left(\frac{\partial \boldsymbol{\mu}}{\partial \xi_j} \right) \right\}}_{h_{ij} :=} \right], \end{aligned} \quad (\text{A11})$$

a. Preliminaries toward deriving \mathbf{J}_D

The partial derivatives in Eq. (A11) are given below,

$$\begin{aligned} \frac{\partial \gamma_{\ell}}{\partial \theta} &= \frac{2\pi}{\lambda} \left[\cos(\theta) \cos(\phi) \Delta_{x,\ell} + \cos(\theta) \sin(\phi) \Delta_{y,\ell} \right. \\ &\quad \left. - \sin(\theta) \left((\ell - 1)D + \Delta_{\parallel,\ell} \right) \right], \end{aligned}$$

$$\frac{\partial \gamma_{\ell}}{\partial \Delta_{x,\ell}} = \frac{2\pi}{\lambda} \sin(\theta) \cos(\phi),$$

$$\frac{\partial \gamma_\ell}{\partial \Delta_{y,\ell}} = \frac{2\pi}{\lambda} \sin(\theta) \sin(\phi),$$

$$\frac{\partial \gamma_\ell}{\partial \Delta_{\parallel,\ell}} = \frac{2\pi}{\lambda} \cos(\theta),$$

$$\frac{\partial \gamma_\ell}{\partial \Delta_{x,m}} = \frac{\partial \gamma_\ell}{\partial \Delta_{y,m}} = \frac{\partial \gamma_\ell}{\partial \Delta_{\parallel,m}} = 0, \quad \forall m \neq \ell,$$

$$\begin{aligned} \frac{\partial [\mathbf{a}]_\ell}{\partial \theta} &= j \frac{\partial \gamma_\ell}{\partial \theta} e^{j\gamma_\ell} \\ &= j \frac{2\pi}{\lambda} [\cos(\theta) \cos(\phi) \Delta_{x,\ell} + \cos(\theta) \sin(\phi) \Delta_{y,\ell} \\ &\quad - \sin(\theta) ((\ell - 1)D + \Delta_{\parallel,\ell})] e^{j\gamma_\ell}, \end{aligned}$$

$$\frac{\partial [\mathbf{a}]_\ell}{\partial \Delta_{x,\ell}} = j \frac{\partial \gamma_\ell}{\partial \Delta_{x,\ell}} e^{j\gamma_\ell} = j \frac{2\pi}{\lambda} \sin(\theta) \cos(\phi) e^{j\gamma_\ell},$$

$$\begin{aligned} \frac{\partial [\mathbf{a}]_\ell}{\partial \Delta_{y,\ell}} &= j \frac{\partial \gamma_\ell}{\partial \Delta_{y,\ell}} e^{j\gamma_\ell} \\ &= j \frac{2\pi}{\lambda} \sin(\theta) \sin(\phi) e^{j\gamma_\ell}, \end{aligned}$$

$$\begin{aligned} \frac{\partial [\mathbf{a}]_\ell}{\partial \Delta_{\parallel,\ell}} &= j \frac{\partial \gamma_\ell}{\partial \Delta_{\parallel,\ell}} e^{j\gamma_\ell} \\ &= j \frac{2\pi}{\lambda} \cos(\theta) e^{j\gamma_\ell}, \end{aligned}$$

$$\frac{\partial [\mathbf{a}]_\ell}{\partial \Delta_{x,m}} = \frac{\partial [\mathbf{a}]_\ell}{\partial \Delta_{y,m}} = \frac{\partial [\mathbf{a}]_\ell}{\partial \Delta_{\parallel,m}} = 0, \quad \forall m \neq \ell.$$

Thus,

$$\frac{\partial \boldsymbol{\mu}}{\partial \boldsymbol{\Delta}} = \mathbf{s} \otimes \frac{\partial \mathbf{a}}{\partial \boldsymbol{\Delta}} = j \frac{2\pi}{\lambda} \mathbf{s} \otimes [\sin(\theta) \cos(\phi), \sin(\theta) \sin(\phi), \cos(\theta)] \otimes \text{diag}[e^{j\gamma_1}, e^{j\gamma_2}, \dots, e^{j\gamma_L}].$$

$$\frac{\partial \boldsymbol{\mu}}{\partial \theta} = \mathbf{s} \otimes \frac{\partial \mathbf{a}}{\partial \theta} = j \frac{2\pi}{\lambda} \mathbf{s} \otimes \begin{bmatrix} (\cos(\theta) \cos(\phi) \Delta_{x,1} + \cos(\theta) \sin(\phi) \Delta_{y,1} - \sin(\theta) \Delta_{\parallel,1}) e^{j\gamma_1} \\ (\cos(\theta) \cos(\phi) \Delta_{x,2} + \cos(\theta) \sin(\phi) \Delta_{y,2} - \sin(\theta) (D + \Delta_{\parallel,2})) e^{j\gamma_2} \\ \vdots \\ (\Delta_{x,L} \cos(\theta) \cos(\phi) + \Delta_{y,L} \cos(\theta) \sin(\phi) - (D(L-1) + \Delta_{\parallel,L}) \sin(\theta)) e^{j\gamma_L} \end{bmatrix}.$$

Using Eq. (A11),

$$h_{\theta,0} = \frac{4M\sigma_s^2\pi^2}{\lambda^2} \sum_{\ell=1}^L \left[\cos(\theta) \cos(\phi) \Delta_{x,\ell} + \cos(\theta) \sin(\phi) \Delta_{y,\ell} - \sin(\theta) (D(\ell-1) + \Delta_{\parallel,\ell}) \right]^2,$$

$$\begin{aligned} \mathbf{h}_{\theta,\Delta} &= \frac{4M\sigma_s^2\pi^2}{\lambda^2} [\sin(\theta) \cos(\phi), \sin(\theta) \sin(\phi), \cos(\theta)] \\ &\quad \otimes \begin{bmatrix} (\cos(\theta) \cos(\phi) \Delta_{x,1} + \cos(\theta) \sin(\phi) \Delta_{y,1} - \sin(\theta) \Delta_{\parallel,1}) \\ (\cos(\theta) \cos(\phi) \Delta_{x,2} + \cos(\theta) \sin(\phi) \Delta_{y,2} - \sin(\theta) (D + \Delta_{\parallel,2})) \\ \vdots \\ (\cos(\theta) \cos(\phi) \Delta_{x,L} + \cos(\theta) \sin(\phi) \Delta_{y,L} - \sin(\theta) (D(L-1) + \Delta_{\parallel,L})) \end{bmatrix}^T = \mathbf{h}_{\Delta,\theta}^T, \end{aligned}$$

$$\mathbf{h}_{\phi,\Delta} = \frac{4M\sigma_s^2\pi^2}{\lambda^2} [\sin(\theta) \cos(\phi), \sin(\theta) \sin(\phi), \cos(\theta)] \otimes \begin{bmatrix} (\cos(\phi) \Delta_{y,1} - \sin(\phi) \Delta_{x,1}) e^{j\gamma_1} \\ (\cos(\phi) \Delta_{y,2} - \sin(\phi) \Delta_{x,2}) e^{j\gamma_2} \\ \vdots \\ (\cos(\phi) \Delta_{y,L} - \sin(\phi) \Delta_{x,L}) e^{j\gamma_L} \end{bmatrix}^T = \mathbf{h}_{\Delta,\phi}^T,$$

$$\mathbf{h}_{\Lambda,\Lambda} = M \left(2\pi \frac{\sigma_s}{\lambda} \right)^2 \begin{bmatrix} \sin^2(\theta) \cos^2(\phi) & \frac{1}{2} \sin^2(\theta) \sin(2\phi) & \frac{1}{2} \cos(\phi) \sin(2\theta) \\ \frac{1}{2} \sin^2(\theta) \sin(2\phi) & \sin^2(\theta) \sin^2(\phi) & \frac{1}{2} \sin(\phi) \sin(2\theta) \\ \frac{1}{2} \cos(\phi) \sin(2\theta) & \frac{1}{2} \sin(\phi) \sin(2\theta) & \cos^2(\theta) \end{bmatrix} \otimes \mathbf{I}_{L \times L}.$$

b. Deriving the entries in the $(3L+1) \times (3L+1)$ matrix of \mathbf{J}_D

Using Eq. (A11),

$$\begin{aligned}
 [\mathbf{J}_D]_{\theta,\theta} &= 8M \left(\frac{\sigma_s \pi}{\lambda \sigma_n} \right)^2 \sum_{\ell=1}^L E_{\Delta} \left[\cos(\theta) (\cos(\phi) \Delta_{x,\ell} + \sin(\phi) \Delta_{y,\ell}) - \sin(\theta) (D(\ell-1) + \Delta_{\parallel,\ell}) \right]^2 \\
 &= 8M \left(\frac{\sigma_s \pi}{\lambda \sigma_n} \right)^2 \sum_{\ell=1}^L \left[\sigma_{\Delta\perp}^2 \cos^2(\theta) + \sin^2(\theta) (\sigma_{\Delta\parallel}^2 + D^2(\ell-1)^2) \right] \\
 &= 8M \left(\frac{\sigma_s \pi}{\lambda \sigma_n} \right)^2 \left[\sigma_{\Delta\perp}^2 L \cos^2(\theta) + \sin^2(\theta) \left(L \sigma_{\Delta\parallel}^2 + D^2 \sum_{\ell=1}^L (\ell-1)^2 \right) \right] \\
 &= 8M \left(\frac{\sigma_s \pi}{\lambda \sigma_n} \right)^2 \left[\sigma_{\Delta\perp}^2 L \cos^2(\theta) + \sin^2(\theta) \left(L \sigma_{\Delta\parallel}^2 + \frac{D^2 L(L-1)(2L-1)}{6} \right) \right] \\
 &= \frac{4ML}{3} \left(\frac{\sigma_s \pi}{\lambda \sigma_n} \right)^2 \left[6\sigma_{\Delta\perp}^2 \cos^2(\theta) + \sin^2(\theta) (6\sigma_{\Delta\parallel}^2 + D^2(L-1)(2L-1)) \right], \\
 [\mathbf{J}_D]_{\theta,\Delta} &= 8M \left(\frac{\sigma_s \pi}{\lambda \sigma_n} \right)^2 [\sin(\theta) \cos(\phi), \sin(\theta) \sin(\phi), \cos(\theta)] \\
 &\quad \otimes E_{\Delta} \begin{bmatrix} \cos(\theta) \cos(\phi) \Delta_{x,1} + \cos(\theta) \sin(\phi) \Delta_{y,1} - \sin(\theta) \Delta_{\parallel,1} \\ \cos(\theta) \cos(\phi) \Delta_{x,2} + \cos(\theta) \sin(\phi) \Delta_{y,2} - \sin(\theta) (D + \Delta_{\parallel,2}) \\ \vdots \\ \cos(\theta) \cos(\phi) \Delta_{x,L} + \cos(\theta) \sin(\phi) \Delta_{y,L} - \sin(\theta) (D(L-1) + \Delta_{\parallel,L}) \end{bmatrix}^T \\
 &= [\sin(\theta) \cos(\phi), \sin(\theta) \sin(\phi), \cos(\theta)] \otimes (-8MD) \sin(\theta) \left(\frac{\sigma_s \pi}{\lambda \sigma_n} \right)^2 [0, 1, \dots, L-1] \\
 &= [\mathbf{J}_D]_{\Delta,\theta}^T, \\
 [\mathbf{J}_D]_{\Delta,\Delta} &= 2M \left(\frac{2\pi \sigma_s}{\lambda \sigma_n} \right)^2 \begin{bmatrix} \sin^2(\theta) \cos^2(\phi) & \frac{1}{2} \sin^2(\theta) \sin(2\phi) & \frac{1}{2} \cos(\phi) \sin(2\theta) \\ \frac{1}{2} \sin^2(\theta) \sin(2\phi) & \sin^2(\theta) \sin^2(\phi) & \frac{1}{2} \sin(\phi) \sin(2\theta) \\ \frac{1}{2} \cos(\phi) \sin(2\theta) & \frac{1}{2} \sin(\phi) \sin(2\theta) & \cos^2(\theta) \end{bmatrix} \otimes \mathbf{I}_{L \times L}.
 \end{aligned}$$

c. The entries of the $(3L+1) \times (3L+1)$ hybrid Fisher information matrix \mathbf{J}

Using Eq. (A6), the hybrid Fisher information matrix is

$$\mathbf{J} = \begin{bmatrix} J_{\theta,\theta} & \mathbf{J}_{\theta,\Delta} \\ \mathbf{J}_{\Delta,\theta} & \mathbf{J}_{\Delta,\Delta} \end{bmatrix},$$

where

$$\begin{aligned}
 J_{\theta,\theta} &= \frac{4ML}{3} \left(\frac{\sigma_s \pi}{\lambda \sigma_n} \right)^2 \left[6\sigma_{\Delta\perp}^2 \cos^2(\theta) + \sin^2(\theta) (6\sigma_{\Delta\parallel}^2 + D^2(L-1)(2L-1)) \right], \\
 \mathbf{J}_{\theta,\Delta} &= -8MD \sin(\theta) \left(\frac{\sigma_s \pi}{\lambda \sigma_n} \right)^2 [\sin(\theta) \cos(\phi), \sin(\theta) \sin(\phi), \cos(\theta)] \otimes [0, 1, \dots, L-1] = \mathbf{J}_{\Delta,\theta}^T,
 \end{aligned}$$

5. The expression of the hybrid Cramér-Rao bound

The hybrid Cramér-Rao bound of the polar angle θ would be given by the first diagonal element of the inverse of \mathbf{J} . The first diagonal entry of \mathbf{J}^{-1} equals [Lu and Shiou, 2002, Eq. (2.3), p. 120]

$$\begin{aligned}
 [\mathbf{J}^{-1}]_{1,1} &= \left(J_{\theta,\theta} - \mathbf{J}_{\theta,\Delta} \mathbf{J}_{\Delta,\Delta}^{-1} \mathbf{J}_{\Delta,\theta} \right)^{-1}, \\
 \mathbf{J}_{\theta,\Delta} \mathbf{J}_{\Delta,\Delta}^{-1} \mathbf{J}_{\Delta,\theta} &= -8MD \sin(\theta) \left(\frac{\sigma_s \pi}{\lambda \sigma_n} \right)^2 \begin{bmatrix} \sin(\theta) \cos(\phi) & \sin(\theta) \sin(\phi) & \cos(\theta) \end{bmatrix} \otimes [0, 1, \dots, L-1] \frac{1}{8M} \left(\frac{\lambda \sigma_n}{\sigma_s \pi} \right)^2 \\
 &\quad \begin{bmatrix} \sin^2(\theta) \cos^2(\phi) + \frac{1}{8M} \left(\frac{\lambda \sigma_n}{\sigma_s \pi \sigma_{\Delta_\perp}} \right)^2 & \frac{1}{2} \sin^2(\theta) \sin(2\phi) & \frac{1}{2} \cos(\phi) \sin(2\theta) \\ \frac{1}{2} \sin^2(\theta) \sin(2\phi) & \sin^2(\theta) \sin^2(\phi) + \frac{1}{8M} \left(\frac{\lambda \sigma_n}{\sigma_s \pi \sigma_{\Delta_\perp}} \right)^2 & \frac{1}{2} \sin(\phi) \sin(2\theta) \\ \frac{1}{2} \cos(\phi) \sin(2\theta) & \frac{1}{2} \sin(\phi) \sin(2\theta) & \cos^2(\theta) + \frac{1}{8M} \left(\frac{\lambda \sigma_n}{\sigma_s \pi \sigma_{\Delta_\parallel}} \right)^2 \end{bmatrix}^{-1} \otimes \mathbf{I}_{L \times L} \\
 &\quad (-8MD) \sin(\theta) \left(\frac{\sigma_s \pi}{\lambda \sigma_n} \right)^2 \begin{bmatrix} \sin(\theta) \cos(\phi) & \sin(\theta) \sin(\phi) & \cos(\theta) \end{bmatrix}^T \otimes [0, 1, \dots, L-1]^T \\
 &= 8M \left(\frac{\sigma_s \pi}{\lambda \sigma_n} D \sin(\theta) \right)^2 \begin{bmatrix} \sin(\theta) \cos(\phi) \sin(\theta) \sin(\phi) \cos(\theta) \end{bmatrix} \\
 &\quad \begin{bmatrix} \sin^2(\theta) \cos^2(\phi) + \frac{1}{8M} \left(\frac{\lambda \sigma_n}{\sigma_s \pi \sigma_{\Delta_\perp}} \right)^2 & \frac{1}{2} \sin^2(\theta) \sin(2\phi) & \frac{1}{2} \cos(\phi) \sin(2\theta) \\ \frac{1}{2} \sin^2(\theta) \sin(2\phi) & \sin^2(\theta) \sin^2(\phi) + \frac{1}{8M} \left(\frac{\lambda \sigma_n}{\sigma_s \pi \sigma_{\Delta_\perp}} \right)^2 & \frac{1}{2} \sin(\phi) \sin(2\theta) \\ \frac{1}{2} \cos(\phi) \sin(2\theta) & \frac{1}{2} \sin(\phi) \sin(2\theta) & \cos^2(\theta) + \frac{1}{8M} \left(\frac{\lambda \sigma_n}{\sigma_s \pi \sigma_{\Delta_\parallel}} \right)^2 \end{bmatrix}^{-1} \\
 &\quad \begin{bmatrix} \sin(\theta) \cos(\phi) & \sin(\theta) \sin(\phi) \cos(\theta) \end{bmatrix}^T [0, 1, \dots, L-1] [0, 1, \dots, L-1]^T \\
 &= 8M \left(\frac{\sigma_s \pi}{\lambda \sigma_n} D \sin(\theta) \right)^2 \frac{\sigma_{\Delta_\perp}^2 \sin^2(\theta) + \sigma_{\Delta_\parallel}^2 \cos^2(\theta)}{\sigma_{\Delta_\perp}^2 \sin^2(\theta) + \sigma_{\Delta_\parallel}^2 \cos^2(\theta) + \frac{1}{8M} \left(\frac{\lambda \sigma_n}{\sigma_s \pi} \right)^2 \sum_{\ell=1}^L (\ell-1)^2} \\
 &= 8M \left(\frac{\sigma_s \pi}{\lambda \sigma_n} D \sin(\theta) \right)^2 \frac{\sigma_{\Delta_\perp}^2 \sin^2(\theta) + \sigma_{\Delta_\parallel}^2 \cos^2(\theta)}{\sigma_{\Delta_\perp}^2 \sin^2(\theta) + \sigma_{\Delta_\parallel}^2 \cos^2(\theta) + \frac{1}{8M} \left(\frac{\lambda \sigma_n}{\sigma_s \pi} \right)^2} \frac{L(L-1)(2L-1)}{6} \\
 &= \frac{4ML}{3} \left(\frac{\sigma_s \pi}{\lambda \sigma_n} \right)^2 \frac{D^2 \sin^2 \theta (L-1)(2L-1) (\sigma_{\Delta_\perp}^2 \sin^2(\theta) + \sigma_{\Delta_\parallel}^2 \cos^2(\theta))}{\sigma_{\Delta_\perp}^2 \sin^2(\theta) + \sigma_{\Delta_\parallel}^2 \cos^2(\theta) + \frac{1}{8M} \left(\frac{\lambda \sigma_n}{\sigma_s \pi} \right)^2}, \tag{A12} \\
 (J_{\theta,\theta} - \mathbf{J}_{\theta,\Delta} \mathbf{J}_{\Delta,\Delta}^{-1} \mathbf{J}_{\Delta,\theta})^{-1} &= \frac{4ML}{3} \left(\frac{\sigma_s \pi}{\lambda \sigma_n} \right)^2 \frac{6\sigma_{\Delta_\perp}^2 \cos^2(\theta) + \sin^2(\theta) [6\sigma_{\Delta_\parallel}^2 + D^2(L-1)(2L-1)]}{\sigma_{\Delta_\perp}^2 \sin^2(\theta) + \sigma_{\Delta_\parallel}^2 \cos^2(\theta) + \frac{1}{8M} \left(\frac{\lambda \sigma_n}{\sigma_s \pi} \right)^2} \\
 &\quad - \frac{4ML}{3} \left(\frac{\sigma_s \pi}{\lambda \sigma_n} \right)^2 \frac{2D^2 \sin^2 \theta (L-1)(2L-1) (\sigma_{\Delta_\perp}^2 \sin^2(\theta) + \sigma_{\Delta_\parallel}^2 \cos^2(\theta))}{\sigma_{\Delta_\perp}^2 \sin^2(\theta) + \sigma_{\Delta_\parallel}^2 \cos^2(\theta) + \frac{1}{8M} \left(\frac{\lambda \sigma_n}{\sigma_s \pi} \right)^2} \\
 &= \frac{4ML}{3} \left(\frac{\sigma_s \pi}{\lambda \sigma_n} \right)^2 \frac{6\sigma_{\Delta_\perp}^2 \cos^2(\theta) + 6\sigma_{\Delta_\parallel}^2 \sin^2(\theta) + \frac{D^2 \sin^2(\theta) (L-1)(2L-1) \lambda^2 \sigma_n^2}{8M \sigma_s^2 \pi^2 [\sigma_{\Delta_\perp}^2 \sin^2(\theta) + \sigma_{\Delta_\parallel}^2 \cos^2(\theta)] + \lambda^2 \sigma_n^2}}{\sigma_{\Delta_\perp}^2 \sin^2(\theta) + \sigma_{\Delta_\parallel}^2 \cos^2(\theta) + \frac{1}{8M} \left(\frac{\lambda \sigma_n}{\sigma_s \pi} \right)^2}. \tag{A13} \\
 (J_{\theta,\theta} - \mathbf{J}_{\theta,\Delta} \mathbf{J}_{\Delta,\Delta}^{-1} \mathbf{J}_{\Delta,\theta})^{-1} &= \frac{3}{4ML} \left(\frac{\sigma_s \pi}{\lambda \sigma_n} \right)^{-2} \frac{1}{6\sigma_{\Delta_\perp}^2 \cos^2(\theta) + 6\sigma_{\Delta_\parallel}^2 \sin^2(\theta) + \frac{D^2 \sin^2(\theta) (L-1)(2L-1) \lambda^2 \sigma_n^2}{8M \sigma_s^2 \pi^2 [\sigma_{\Delta_\perp}^2 \sin^2(\theta) + \sigma_{\Delta_\parallel}^2 \cos^2(\theta)] + \lambda^2 \sigma_n^2}}, \\
 \text{HCRB}_{\parallel,\perp}(\theta) &= \left[\frac{4ML}{3} \left(\frac{\sigma_s \pi}{\lambda \sigma_n} \right)^2 \left(6\sigma_{\Delta_\perp}^2 \cos^2(\theta) + 6\sigma_{\Delta_\parallel}^2 \sin^2(\theta) + \frac{D^2 \sin^2(\theta) (L-1)(2L-1) \lambda^2 \sigma_n^2}{8M \sigma_s^2 \pi^2 [\sigma_{\Delta_\perp}^2 \sin^2(\theta) + \sigma_{\Delta_\parallel}^2 \cos^2(\theta)] + \lambda^2 \sigma_n^2} \right) \right]^{-1}, \tag{A14}
 \end{aligned}$$

which gives Eq. (6).

¹This dislocation model is same as that in [Hinich \(1977\)](#), except that the linear array there is oriented along the x axis, whereas this paper's array is oriented along the z -axis.

²The dislocation model in Eq. (3) is same as that in [Schultheiss and Ianniello \(1980\)](#) and [Wong et al. \(1988\)](#), except that these references orient their linear array along the x axis, but this paper's array is oriented along the z -axis.

³With the fewest possible sensors in the array (i.e., with $L = 2$),

$$\text{HCRB}_{\parallel, \perp}(\theta) = \left\{ 2\text{SNR}_{\text{eff}} \left[2a_{\text{ext}} + \frac{(\frac{D}{\lambda} \sin(\theta))^2}{2\text{SNR}_{\text{eff}} a_{\text{nui}} + 1} \right] \right\}^{-1}$$

⁴At the largest possible value for $(D/\lambda) \sin(\theta)$ under half-wavelength spacing [i.e., at $(D/\lambda) \sin(\theta) = \frac{1}{2}$],

$$\begin{aligned} \text{HCRB}_{\parallel, \perp}(\theta) \\ = \left\{ L\text{SNR}_{\text{eff}} \left[2a_{\text{ext}} + \frac{\frac{1}{2}(L-1)(2L-1)}{2\text{SNR}_{\text{eff}} a_{\text{nui}} + 1} \right] \right\}^{-1} \end{aligned}$$

⁵No prior reference [except [Wan et al. \(2014\)](#)] has recognized this non-monotonic trend with respect to $\sigma_{\Delta_{\parallel}}$ or $\sigma_{\Delta_{\perp}}$, because the dislocations have always been kept very small in these references. Even [Wan et al. \(2014\)](#) offer little explanation.

Aalborg University (2018). "Equipment," <https://www.smdr.es.aau.dk/equipment/> (Last viewed 4/24/2020).

Abdellatif, T., Larzabal, P., and Clergeot, H. (2000). "Performance study of a generalized subspace-based method for scattered sources," in *IEEE International Conference on Acoustics, Speech, and Signal Processing*, Vol. 5, pp. 3101–3104.

Agrawal, M., and Prasad, S. (2000). "A modified likelihood function approach to DOA estimation in the presence of unknown spatially correlated Gaussian noise using a uniform linear array," *IEEE Trans. Sign. Process.* **48**(10), 2743–2749.

Barbagelata, A., Guerrini, P., and Troiano, L. (2008). "Thirty years of towed arrays at NURC," *Oceanography* **21**(2), 24–33.

Bellili, F., Affes, S., and Stephenne, A. (2010). "On the lower performance bounds for DOA estimators from linearly-modulated signals," in *Biennial Symposium on Communications*, pp. 381–386.

Choi, Y. H. (2002). "Alternating minimisation approach to generalised music and its performance," *IEE Proc. Radar Sonar Nav.* **149**(2), 97–101.

Demissie, B., and Willett, P. (2008). "Subspace approach to direction finding of rapidly moving sources with a uniform linear array," in *IEEE Convention of Electrical and Electronics Engineers in Israel*, pp. 664–668.

Fayad, Y., Wang, C., Hafez, A. E. D. S., and Cao, Q. (2014). "Direction of arrival estimation using novel esprit method for localization and tracking radar systems," in *IEEE International Bhurban Conference on Applied Sciences and Technology*, pp. 396–398.

Fittipaldi, D. A., and Luise, M. (2008). "Cramér-Rao bound for DOA estimation with antenna arrays and UWB-OFDM signals for pan applications," in *IEEE International Symposium on Personal, Indoor and Mobile Radio Communications*.

Gershman, A. B., and Bohme, J. F. (1997). "A note on most favorable array geometries for DOA estimation and array interpolation," *IEEE Sign. Process. Lett.* **4**(8), 232–235.

Gershman, A. B., Pesavento, M., and Amin, M. G. (2001). "Estimating parameters of multiple wideband polynomial-phase sources in sensor arrays," *IEEE Trans. Sign. Process.* **49**(12), 2924–2934.

Hinich, M. J. (1977). "Bearing estimation using a perturbed linear array," *J. Acoust. Soc. Am.* **61**(6), 1540–1544.

Hu, Y., Zhou, H., Lu, J., and Qiu, X. (2016). "Effects of a near-field rigid sphere scatterer on the performance of linear microphone array beamformers," *J. Acoust. Soc. Am.* **140**(2), 924–935.

Jing, H., Wang, H., Liu, Z., and Shen, X. (2018). "DOA estimation for underwater target by active detection on virtual time reversal using a uniform linear array," *Sensors* **18**(8), 2458.

JSK Naval Support (2018). "Thin line array," <http://www.jsksnaval.ca/wp-content/uploads/2015/10/Thin-Line-Array.pdf> (Last viewed 4/24/2020).

Kaneko, K., and Sano, A. (2008). "Music-like iterative DOA estimation in multipath environments," in *Sensor Array and Multichannel Signal Processing Workshop*, pp. 212–215.

Kautz, G. M., and Zoltowski, M. D. (1996). "Beamspace DOA estimation featuring multirate eigenvector processing," *IEEE Trans. Sign. Process.* **44**(7), 1765–1778.

Leshem, A., and der Veen, A.-J. V. (1999). "Direction-of-arrival estimation for constant modulus signals," *IEEE Trans. Sign. Process.* **47**(11), 3125–3129.

Li, J., and Compton, R. T., Jr. (1991). "Maximum likelihood estimation of the arrival direction of a signal with known waveform," in *IEEE International Conference on Systems Engineering*.

Li, M., and Lu, Y. (2007). "Maximum likelihood processing for arrays with partially unknown sensor gains and phases," in *7th International Conference on Telecommunications*, pp. 1–6.

Li, M., Yilong, L., and He, B. (2013). "Array signal processing for maximum likelihood direction-of-arrival estimation," *J. Electr. Electr. Syst.* **3**(1), 117.

Lu, T. T., and Shiou, S. H. (2002). "Inverses of 2×2 block matrices," *Comput. Math. Appl.* **43**, 119–129.

Noam, Y., and Messer, H. (2009). "Notes on the tightness of the hybrid Cramér-Rao lower bound," *IEEE Trans. Sign. Process.* **57**(6), 2074–2084.

Ottersten, B., Viberg, M., and Kailath, T. (1991). "Performance analysis of the total least squares esprit algorithm," *IEEE Trans. Sign. Process.* **39**(5), 1122–1135.

Schultheiss, P. M., and Ianniello, J. P. (1980). "Optimum range and bearing estimation with randomly perturbed arrays," *J. Acoust. Soc. Am.* **68**(11), 167–173.

Stoica, P., and Nehorai, A. (1989). "Music, maximum likelihood, and Cramér-Rao bound," *IEEE Trans. Acoust. Speech Sign. Process.* **37**(5), 720–741.

Tayem, N., Omer, M., and Hussain, A. A. (2014). "Hardware implementation of music and esprit on NI-PXI platform," in *IEEE Military Communications Conference*, pp. 329–332.

Tichavsky, P., and Wong, K. T. (2004). "Quasi-fluid-mechanics-based quasi-Bayesian Cramér-Rao bounds for deformed towed-array direction-finding," *IEEE Trans. Sign. Process.* **52**(1), 36–47.

Tuncer, T. E., and Friedlander, B. (2009). *Classical and Modern Direction-of-Arrival Estimation*.

University of Pretoria (2018). "Research," <https://www.up.ac.za/en/sentech-chair-in-broadband-wireless-multimedia-communication/article/1953124/research> (Last viewed 4/24/2020).

VanTrees, H. L. (2002). *Optimum Array Processing: Part IV of Detection, Estimation and Modulation Theory*.

VanTrees, H. L., and Bell, K. L. (2007). *Bayesian Bounds for Parameter Estimation and Nonlinear Filtering/Tracking*.

Wan, S., Tang, J., Zhu, W., and Zhang, N. (2014). "Identifiability analysis for array shape self-calibration based on hybrid Cramér-Rao bound," *IEEE Sign. Process. Lett.* **21**(4), 473–477.

Wong, K. M., Walker, R. S., and Niezgoda, G. (1988). "Effects of random sensor motion on bearing estimation by the music algorithm," *IEE Proc. Radar Sign. Process.* **135**(3), 233–250.

Xia, W., He, Z., and Liao, Y. (2007). "Subspace-based method for multiple-target localization using MIMO radars," in *IEEE International Symposium on Signal Processing and Information Technology*, pp. 715–720.

XMOS (2018). "VocalFusion speaker product brief," <http://www.xmos.com/tw/support/boards?product=35855> (Last viewed 4/24/2020).

Ye, H., and DeGroat, R. D. (1993). "Maximum likelihood DOA and unknown colored noise estimation with asymptotic Cramér-Rao bounds," in *IEEE Asilomar Conference on Signals, Systems and Computers*, pp. 1391–1395.

Ye, H., and DeGroat, R. D. (1995). "Maximum likelihood DOA estimation and asymptotic Cramér-Rao bounds for additive unknown colored noise," *IEEE Trans. Sign. Process.* **43**(4), 938–949.

Zatman, M. (1998). "Properties and applications of wideband Cramér-Rao bounds," in *IEEE Workshop on Statistical Signal and Array Processing*, pp. 41–44.

Zhenghui, G., and Gunawan, E. (2000). "Cramér-Rao bound for joint direction of arrival, time delay estimation in DS-CDMA systems," in *IEEE Military Communications Conference*, pp. 614–618.